Conjugate heat transfer numerical study of the ejector by means of SU2 solver

Conjugate heat transfer numerical study of the ejector by means of SU2 solver

D V Brezgin [1], K E Aronson [1], F Mazzelli [2], A Milazzo [2]

[1] Ural Federal University - UrFU, Mira str., 19, Ekaterinburg, 620002, Russia
[2] University of Florence, S. Marco str., 4, Florence, 50121, Italy

dvbrezgin@urfu.ru

Abstract. In this paper, the test supersonic ejector with conjugate heat transfer in solid bodies has been studied numerically. An extensive numerical campaign by means of open-source SU2 solver is performed to analyze the fluid dynamics of the ejector flowfield accounting for the heat conduction in solids. The fluid domain simulation is carried out by employing compressible RANS treatment whilst the heat distribution in solids is predicted by simultaneous solving the steady heat conduction equation. The working fluid is R245fa and all simulations are performed accounting for real gas properties of the refrigerant. Experimental data against numerical results comparison showed close agreement both in terms mass flow rates and static pressure distribution along the walls. Within the CFD trials, the most valuable flow parameters at a wall vicinity are compared: distribution across the boundary layer of the temperature and the turbulent kinetic energy specific dissipation rate, boundary layer displacement and momentum thicknesses. A comprehensive analysis of the simulation results cases with adiabatic walls against cases with heat permeable walls revealed the actual differences of the flow properties in the wall vicinity. However, the ejector performance has not changed noticeably while accounting for the heat conduction in solids.

1. Introduction

Ejectors are widely used in refrigeration since their ability to utilize low temperature heat to produce cooling. As any jet pump, ejector's design consists of two main parts: motive or primary nozzle and diffuser, which combines the mixing chamber and diffuser section. In motive nozzle, the potential energy of the primary flow is converted into kinetic energy of the jet (momentum). Further downstream in the ejector's mixing chamber, the supersonic primary flow involves a static secondary flow through a turbulent interaction in the free shear layer. The bulk momentum of the mixed flows determines the backpressure upper limit value, which the ejector is able to overcome without loss in performance. In general, the performance of an ejector is determined as the *Entrainment Ratio* '***Er***' (the secondary to the primary mass flow rates ratio) and, in "on-design" mode, it doesn't depend on the discharge pressure value while it's below the critical one.

In recent years, an interest to the ejectors simulations by employing various commercial and open-source CFD solvers is greatly increased. However, most of the studies are carried out by assuming adiabatic walls, thereby limiting both the numerical results accuracy and the power of applicability of any CFD tool. The latter outcome stems from the fact that no other kind of research method lets predict forced heat transfer with such a little effort as a CFD modeling. Study in Ref [1] is an exception from

the general trend, where authors investigate the heat transfer process within the CO_2 two-phase ejector. The numerical simulations presented in Ref [1] were carried out with the non-adiabatic inner walls and the insulated outer walls of the ejector. The numerical results comparison had led to significant decrease in Entrainment ratio (about 15%) for the non-adiabatic wall cases. In despite of such noticeable contradiction of numerical results for distinct wall model cases, no subsequent analysis was performed. Moreover, assuming insulated outer walls does not make sense in terms of conjugate heat transfer modeling because of the fact that such kind of steady state simulation will suffer either from convergence issues or will lead to the same adiabatic wall results by the end.

Fluid mechanics theory for compressible viscous flows unambiguously shows that components of the viscous stress tensor act like prevail heat sources within conservation energy equation in the boundary layer where the largest velocity gradients take place. As a result, in some particular high Mach number flows, the enthalpy difference within boundary layer between adiabatic and real (non-adiabatic) walls may cause significant deviation. At that, in a coupled iterative solution it leads to all conservative quantities alteration and changes in numerical results accuracy. Therefore, accurate prediction of the high-speed flows requires imposing heat permeable walls where conjugate heat transfer through the strong boundaries is preferable solution because of CFD solution set-up flexibility.

The present research builds on work in Ref [2] and extends it in terms of conjugate heat transfer modeling by means of the open-source SU2 CFD solver. The major features and capabilities of the open-source SU2 tool are described in details in Ref [3] whilst the description of the test rig ejector chiller and experimental data acquisition is held in Ref [2]. Although most part of the study in Ref [2] is concerned to numerical simulations as well, the present research had not set a task to make a comparison of the distinct numerical solvers, approaches and the results. The present research aim is to compare the ejector‘s performance by means of two distinct numerical modeling approaches: adiabatic and heat permeable walls as well as evaluate fluid flow features in the vicinity of solid walls.

2. Numerical model

The numerical fluid model in this study is based on compressible RANS solver whilst the single heat equation is utilized for solving temperature distribution in solid bodies. At that, the standard approach is used in which the heat fluxes from the fluid domain are exposed to the solid boundaries through prescribed interface pairs. The governing equation for conservation of mass, radial momentum, axial momentum and total energy of the fluid domain in 2D axisymmetric form can be written as,

$$
\begin{aligned}
&\frac{\partial \rho}{\partial t}+\frac{\partial \rho v_r}{\partial r}+\frac{\partial \rho v_z}{\partial z}=-\frac{\rho v_r}{r}\\
&\frac{\partial \rho v_r}{\partial t}+\frac{\partial \rho v_r^2+p}{\partial r}-\frac{\partial}{\partial r}\left[\mu_{eff}\left(2\frac{\partial v_r}{\partial r}-\frac{2}{3}\left(\frac{\partial v_z}{\partial z}+\frac{\partial v_r}{\partial r}\right)+\frac{2}{3}\rho k\right)\right]+\frac{\partial \rho v_r v_z}{\partial z}-\frac{\partial}{\partial z}\left[\mu_{eff}\left(\frac{\partial v_z}{\partial r}+\frac{\partial v_r}{\partial z}\right)\right]=\\
&\qquad -\frac{\rho v_r^2}{r}+\frac{4\mu_{eff}}{3}\left(\frac{1}{r}\frac{\partial v_r}{\partial r}-\frac{v_r}{r^2}\right)\\
&\frac{\partial \rho v_z}{\partial t}+\frac{\partial \rho v_r v_z}{\partial r}-\frac{\partial}{\partial r}\left[\mu_{eff}\left(\frac{\partial v_z}{\partial r}+\frac{\partial v_r}{\partial z}\right)\right]+\frac{\partial \rho v_z^2+p}{\partial z}-\frac{\partial}{\partial z}\left[\mu_{eff}\left(2\frac{\partial v_z}{\partial z}-\frac{2}{3}\left(\frac{\partial v_z}{\partial z}+\frac{\partial v_r}{\partial r}\right)+\frac{2}{3}\rho k\right)\right]=\\
&\qquad -\frac{\rho v_r v_z}{r}+\frac{\mu_{eff}}{r}\left(\frac{1}{3}\frac{\partial v_r}{\partial z}-\frac{\partial v_z}{\partial r}\right)\\
&\frac{\partial E_t}{\partial t}+\frac{\partial}{\partial r}\left(v_r(E_t+p)\right)+\frac{\partial}{\partial z}\left(v_z(E_t+p)\right)\\
&\qquad -\frac{\partial}{\partial r}\left\{v_r\left[\mu_{eff}\left(2\frac{\partial v_r}{\partial r}-\frac{2}{3}\left(\frac{\partial v_z}{\partial z}+\frac{\partial v_r}{\partial r}\right)+\frac{2}{3}\rho k\right)\right]+v_z\left[\mu_{eff}\left(\frac{\partial v_z}{\partial r}+\frac{\partial v_r}{\partial z}\right)\right]-k_{eff}\frac{\partial T}{\partial r}\right\}\\
&\qquad -\frac{\partial}{\partial z}\left\{v_z\left[\mu_{eff}\left(2\frac{\partial v_z}{\partial z}-\frac{2}{3}\left(\frac{\partial v_z}{\partial z}+\frac{\partial v_r}{\partial r}\right)+\frac{2}{3}\rho k\right)\right]+v_r\left[\mu_{eff}\left(\frac{\partial v_z}{\partial r}+\frac{\partial v_r}{\partial z}\right)\right]-k_{eff}\frac{\partial T}{\partial z}\right\}\\
&\qquad =\frac{1}{r}\left[-v_r(E_t+p)+\mu_{eff}\left(v_z\frac{\partial v_z}{\partial r}+\frac{v_z}{3}\frac{\partial v_r}{\partial z}-\frac{4v_r}{3}\frac{\partial v_z}{\partial z}+\frac{2v_r}{3}\rho k\right)-k_{eff}\frac{\partial T}{\partial r}\right]
\end{aligned}
\tag{1}
$$

, where μ_{eff} and k_{eff} stands for the effective viscosity and effective thermal conductivity, k is the turbulent kinetic energy, ρ is the density, T is the temperature, p is the pressure and the total energy per unit volume E_t is calculated as

$$E_t=\rho\left(e+0.5(v_r^2+v_z^2)\right). \tag{2}$$

As can be seen, all conservative equations in (1) resembles the planar two-dimensional form while the right-hand side part distinguishes the extra terms which are concerned to axisymmetric form only. The eddy viscosity is obtained by employing the standard *Menter's k-ω SST* turbulence model expressed in axisymmetric form as well. Throughout all the simulations, *modified Peng-Robinson equation of state* is used. In order to get more accurate and consistent with the R245fa refrigerant thermodynamic properties, authors altered the built-in implementation of the Peng-Robinson equation of state by deliberately getting rid of using the specific heat ratio within the SU2 solver code routine. At that, the implementation of the cubic pressure-explicit equation of state is extracted from open-source library CoolProp [4], wherein the exact formulation is presented in Ref [5]. The corresponding fixes in the SU2 solver code made it possible to use a spatially variable value of the specific heat capacities, which had a positive effect not only on the accuracy of determining the thermodynamic properties of the fluid but on the solution convergence as well. Laminar viscosity is defined by imposing *Sutherland's model* ($\mu_{ref} = 1.703e-5,\ T_{ref} = 490.7,\ S = 405$), whilst *constant Prandtl* treatment (Pr = 0.71) for the thermal conductivity is employed in numerical solution procedures. Both of the transport models are quite well fitted within the possible temperature range throughout all the simulations.

Inlet boundary conditions of the fluid domain are set by assigning total pressures and temperatures, static pressure condition is set for the diffuser discharge outlet. Solid body's boundaries, which are not in direct contact with the fluid domain, are set by imposing the proper heat fluxes towards the environment.

Convective fluxes in (1) are solved by means of classic *Roe upwind* scheme in conjunction with limiting the proper minimum convective eigenvalue (entropy correction is 0.02). In order to achieve second order upwind accuracy, the *MUSCL* reconstruction is employed with *Venkatakrishnan-Wang slope limiter* to suppress spurious oscillations at the shock regions. Spatial gradient are solved by means of the Green-Gauss node based method, whilst the *FGMRES linear solver* with *ILU preconditioner* is utilized to solve overall *Euler implicit time discretization*.

All the domains (fluid and solids) are discretized by means of structured grid and distinguished by imposing the proper interfaces between each other. At that, the grid properly resolves the boundary layer by adjusting the first cell layer height to make sure that the wall Y+ value < 1.0 along the solid walls and at least 30 cells are placed until boundary layer edge is reached.

In order to get more insight into boundary layer development features, the comprehensive post-process analysis is carried out throughout the present research. In fact, boundary layer displacement and momentum thicknesses along the nozzle and diffuser walls are evaluated. In general, displacement thickness defines the mass flow rate deficit that the real flow undergoes because of viscosity and it measures the hypothetical wall shift along the surface normal that is required to compensate such mass flow rate deficit. Momentum thickness has the similar definition except the fact that is related to momentum flow rate. The exact formulations of these two tools are the following:

$$\delta = \int_0^h \left(1 - \frac{\rho v}{\rho_h v_h}\right) dy, \qquad \theta = \int_0^h \frac{\rho v}{\rho_h v_h}\left(1 - \frac{v}{v_h}\right) dy \tag{3}$$

, where δ is the displacement thickness, θ is the momentum thickness, h denotes the distance from the surface to the boundary layer edge, ρ_h and v_h are the flow density and free stream velocity at the boundary layer edge respectively, while ρ and v are the flow density and velocity perpendicular to surface normal at the wall distance *dy*. In present study, definite integrals (3) are solved numerically and the boundary layer edge is determined by employing a threshold value of the gradient of the turbulent kinetic energy specific dissipation rate (omega). It should be noted, that the exact threshold magnitude of '*omega* gradient' is case dependent and requires additional calculations in advance.

3. Results and discussion

At first, ejector flowfield is simulated with adiabatic walls. After the proper convergence is reached and all the validation steps (mass flow rates comparison and static pressure distribution matching) against the experimental data are successfully met, the next simulation is launched by including the solid

domains and imposing the heat transfer through contacting surfaces. Such kind of approach lets run conjugate heat transfer modeling task from the already converged case of the fluid simulation, which significantly reduces the overall solution time.

A detailed numerical post process campaign has been carried throughout the present research in terms of results comparison for adiabatic and heat permeable (conjugate heat transfer) ejector cases. The description and explanation of the major exposed tools and features are presented hereafter. However, it must be admitted that the performance of the investigated ejector practically does not change when the conjugate heat transfer through solid walls is taking into account. In fact, there is a decrease in the secondary mass flow rate by 0.1%, but such a tiny drop appears to contradict with the results given in Ref [1].

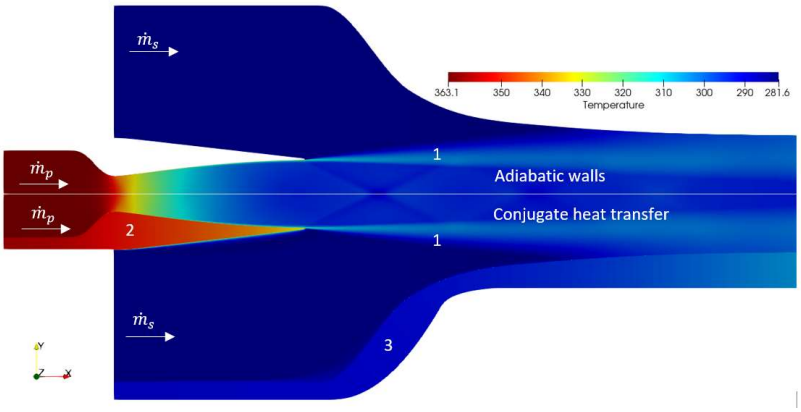

Figure 1. Temperature distribution comparison across the suction and mixing chambers

The most remarkable qualitative results are presented in Figure 1, 2 in which the temperature field distribution of the adiabatic walls case (uppermost part from the ejector centerline) and conjugate heat transfer case is compared. The integer values on the Figure 1 indicate the fluid domain (1), the solid nozzle domain (2) and the solid diffuser domain (3). All three domains are simultaneously solved by multizone SU2 iterative solution.

One may notice that the inlet part of the solid diffuser (#3 in Figure 1) is heated a little bit relatively to the secondary fluid flow (#2 in Figure 1). This phenomenon can be explained by the heat conduction and this process is evident while analyzing Figure 2, where the temperature of the metal in the shock vicinity and the flow temperature just behind the shock are identical. However, the flow temperature ahead of the shock deviates from the solid body temperature at the same cross section, where the solid diffuser is much hotter because of heat flux directed backward.

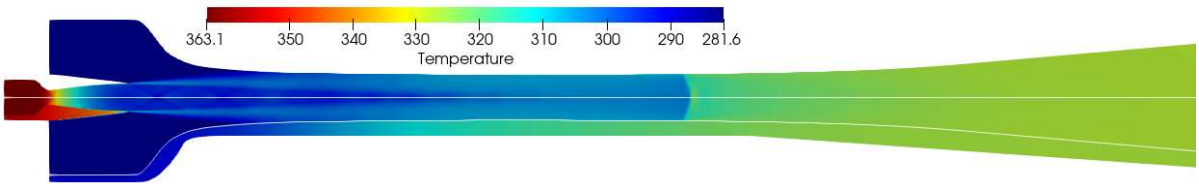

Figure 2. Temperature distribution comparison across the entire ejector: uppermost - adiabatic walls, bottom – conjugate heat transfer

Figure 3 represents the comparison of temperature and turbulent kinetic energy specific dissipation rate (Omega) distribution along the nozzle wall and averaged by integration across the boundary layer height. As can be seen from the Fig.3, the averaged boundary layer temperature is slightly displaced downward in CHT modeling case. In general, these temperature differences have not exceed 2 degrees downstream of the nozzle throat, however, the temperature differences on the solid surfaces itself may exceed 18 degrees.

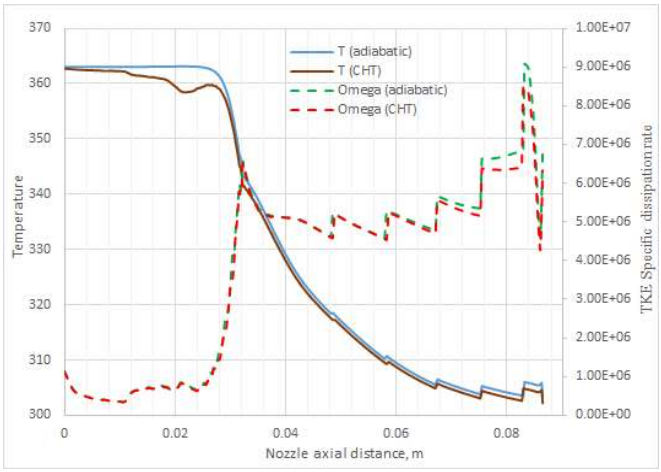

Figure 3. Averaged temperature and TKE specific dissipation rate across the boundary layer

Figure 4 represents the distribution of the boundary layer displacement and momentum thicknesses along the nozzle wall for two distinct cases: adiabatic walls and conjugate heat transfer model (CHT). The boundary layer analysis along the nozzle wall revealed that mass flow deficit, which is concerned to displacement thickness, decreases onto 1% in CHT case, whilst the momentum flux deficit increases up to 2%. Such contradicting results have physical explanation. A decrease in the mass flux deficit in the CHT case is largely associated with the density augmentation near the solid walls, while a velocity drop across the boundary layer causes an increase in the momentum deficit. Anyway, the overall differences between both of cases (adiabatic and CHT) are too negligible to have an impact on downstream flows mixing or ejector performance.

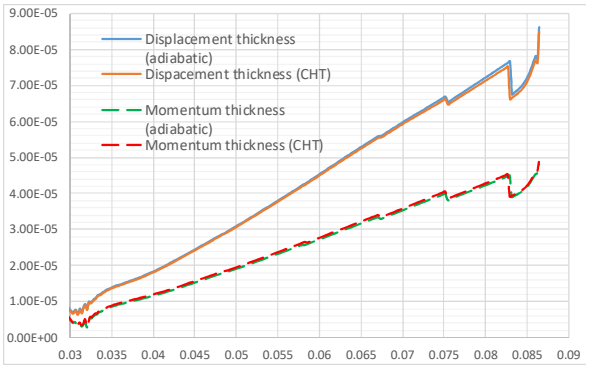

Figure 4. Boundary layer displacement and momentum thicknesses along the nozzle wall

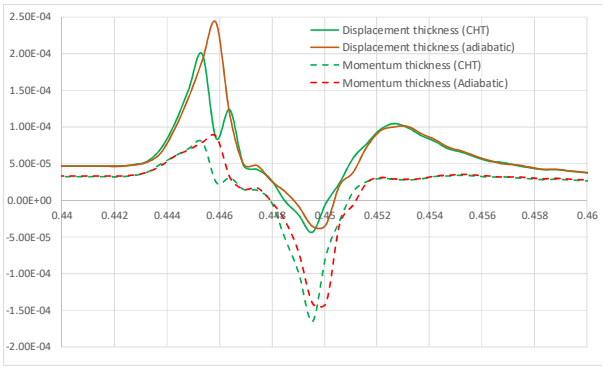

Figure 5. Boundary layer displacement and momentum thicknesses along the diffuser wall in the shock vicinity

Boundary layer along the diffuser wall is evaluated throughout present numerical research as well. It is noticeable that averaged temperature across the boundary layer height in the diffuser suction chamber is greater on 5 degrees for the CHT case, while in the mixing chamber the temperatures as well as displacement and momentum thicknesses are almost identical downstream of both the CHT and adiabatic cases. However, there is a remarkable boundary layer feature along the diffuser wall in the secondary shock vicinity. The shock is caused by the adverse pressure gradient and induces the boundary layer separation with the subsequent flow recirculation zone behind the shock. Figure 5 represents the boundary layer displacement and momentum thicknesses along the diffuser wall in the shock vicinity for two distinct cases: CHT and adiabatic walls. As can be seen from the Fig.5, the boundary layer separation onset is shifted upstream and it literally means that momentum loss caused by the viscous

forces is greater for the CHT modeling case. At the same time, the actual differences in flow behavior between distinguished CHT and adiabatic walls models is negligible.

4. Conclusions:

The study presents the numerical results comparison obtained on supersonic ejector for refrigeration with two distinct models: adiabatic walls and conjugate heat transfer. All the simulation cases are carried out by means of open-source SU2 solver and it's turned out that taking into account the heat transfer through solid wall have negligible impact on overall ejector performance. Moreover, the general tools developed and implemented in SU2 code throughout the present study to estimate local boundary layer flow features (boundary layer displacement and momentum thicknesses) revealed that there is no major differences between both of distinct cases. Definitely, this outcome cannot be carried over to all ejector designs and operation modes. Thus, it is likely that at higher speed flows (with a higher degree of flow expansion in the primary nozzles), viscous stresses in the boundary layer will prevail, and in such a case, it will cause the ejector performance alteration. However, it's well known that flows interaction within the mixing layer as well as the shock train located downstream and caused by the adverse pressure gradient are the main sources of ejector's performance losses. Thereby, all the CFD treatments and efforts within ejector in the scope of the boundary layer model calibrating will fail until the most important domain regions (away from the solid surfaces) is not fully consistent with the actual fluid dynamics.

References:

[1] Haida M et al. 2018 Heat transfer process within the R744 two-phase ejector: numerical and experimental study. *Proc. 17th Int. Refrigeration and Air Conditioning Conf*. (Purdue: Perdue University)
[2] Mazzelli F, Milazzo A 2015 *Int J Refrig* **49** 79-92
[3] Economon T D, Palacios F, Copeland S R, Lukaczyk T W and Alonso J J 2016 *AIAA Journal* **54**(3) 828-846
[4] Bell I H, Wronski J, Quoilin S and Lemort V 2014 *Ind Eng Chem Res* **53**(6) 2498-2508
[5] Bell I H and Jäger A 2016 *J. Res. Nat. Inst. Stand. Technol* **121** 238